

# Entanglement distribution among distinct mechanical nodes in a quantum network

Zhi-Yuan Fan<sup>1,\*</sup> and Liu-Yong Cheng<sup>1,2</sup>

<sup>1</sup>*School of Physics and Electronic Engineering, Shanxi Normal University, Taiyuan, Shanxi 030031, China*

<sup>2</sup>*Institute of Quantum Science and Technology, Yanbian University, Yanji 133002, China*

(Dated: March 12, 2026)

We propose two schemes to achieve remote entanglement distribution between two mechanical nodes with a significant frequency mismatch, based on optomechanical systems. The first scheme utilizes the physical mechanism to redistribute the quantum entanglement initially established in a dispersively-coupled optomechanical system with a megahertz mechanical resonance to a distant optomechanical system which embodies the triple-resonant interaction induced by the scattering of gigahertz mechanical phonon. We also provide a fast optical pulse protocol to realize the long-distance entanglement distribution from the optomechanical system supporting the gigahertz mechanical mode to the megahertz mechanical mode included in a distant optomechanical system. Specifically, these two schemes respectively demonstrate the megahertz-to-gigahertz and gigahertz-to-megahertz entanglement distribution in the quantum network of optical photons and phonons. This work may facilitate the application of various mechanical systems in hybrid quantum network-based quantum technologies and fundamental physical research.

## I. INTRODUCTION

The emergence of hybrid quantum systems highlights the necessity to utilize diverse quantum systems with distinct advantages and complementary functionalities to cooperatively perform the quantum tasks [1–7]. As one indispensable building block, the mechanical systems, which support long lifetime, fabrication flexibility in size and resonance frequency (range from kilohertz to gigahertz), may find broad applications in modern quantum technologies [8, 9]. Therefore, it is of significant importance to possess the ability to manipulate and measure the physical state of different mechanical systems. The study of interactions between light and matter opened up a burgeoning field to achieve this, namely, the cavity optomechanics [10]. Along with the promising progress in micro-nano fabrication, optical manipulation and precision measurement, the nonlinear interaction between photons and mechanical phonons has been demonstrated on a variety of optomechanical physical platforms in recent decades, which enables optical control and readout of the mechanical motions in these hybrid systems. In the quantum regime, the cavity optomechanics has unique application in realizing various kinds of mechanical quantum states on the macroscopic scale [11–29]. With regard to the mechanical entangled states, there has been many schemes in advances of cavity optomechanics [30–42]. Specifically, the experimental demonstration of macroscopic entanglement between a couple of mechanical systems with gigahertz [43] or megahertz [44–46] resonances have been achieved due to their vital important applications in quantum field. The high frequency mechanical systems with gigahertz resonance have an obvious superiority on the robustness against thermal effect and play crucial roles in quantum fundamental test [12, 13], quantum teleportation [14], low noise microwave to optics conversion [47], and quantum computational devices interface [48], etc. The megahertz-resonant mechanical systems, with long coherent

lifetime, also find unique applications in quantum information storing [49], precision measurement [50–52], nonreciprocal device fabrication [53–56], and mechanical phonon lasing [57–59]. In view of this, it is natural to consider combining such two distinct systems and further realizing entanglement or even remote entanglement of two mechanical systems with a significant frequency mismatch, which leads to entanglement distribution between different mechanical nodes in a quantum network. However, up to date, the mechanical entanglement between distinct mechanical nodes [60, 61] or over a long distance [62, 63] has been much less explored, which restricts the wide application of distinct mechanical systems in hybrid quantum network construction and related quantum technologies.

Here, we show that the obstacle can be eliminated and provide two theoretical proposals to achieve the macroscopic entanglement between distinct mechanical nodes. The first scheme mainly employs a hybrid model including two optomechanical systems, which embody mechanical resonances with a significant frequency mismatch, and respectively support dispersive and triple-resonant interactions. In principle, under the pumping of a *strong* red-detuned drive, the quantum entanglement between the optical cavity and megahertz mechanical mode can be activated in the optomechanical system with nonlinear dispersive coupling. Via the mediation of propagating optical photons, such quantum correlation can be further distributed to the gigahertz mechanical node exploiting the Brillouin scattering (BLS)-induced optomechanical state transfer process in the cascaded optomechanical system, thus realizing distant entanglement distribution from megahertz to gigahertz mechanical nodes in the hybrid quantum network. Besides, how to distribute the entanglement from the optomechanical system which includes the gigahertz mechanical node to the remote mechanical node in megahertz range also merits great research interest. To reach this, we give an optical pulse-assisted scheme by successively activate the optomechanical Stokes and anti-Stokes processes. The former achieves quantum entanglement by preparing a two-mode squeezed vacuum state between the gigahertz mechanical node and the optical pulse. Then, the quantum state of the

\* fanzhiyuan@sxnu.edu.cn

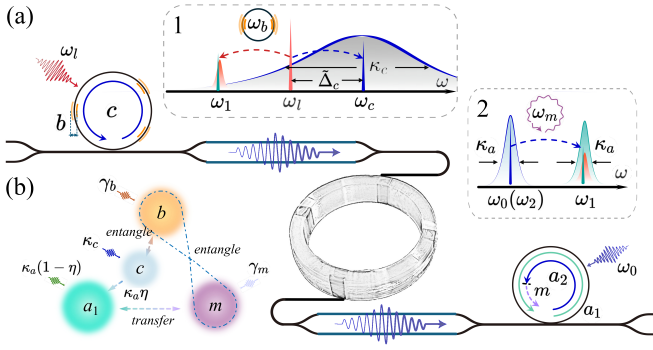


FIG. 1. Schematic diagrams of the (a) hybrid system and (b) physical mechanism to realize the remote megahertz-to-gigahertz mechanical entanglement distribution. Inset 1: Entanglement generation process. The down-conversion sideband ( $\omega_l - \omega_b$ ) of the optical cavity mode ( $c$ ) can couple to the WGM ( $a_1$ ) via the mediation of optical waveguide. Inset 2: Entanglement distribution process. The optical WGM ( $a_2$ ) is resonantly pumped by a laser to activate the beam-splitter type interaction.

travelling temporal mode can be mapped onto the megahertz mechanical node through the state transfer activated by the anti-Stokes scattering in the remote optomechanical system, which establishes a nonlocal entanglement shared by distinct mechanical systems.

## II. REMOTE ENTANGLEMENT DISTRIBUTION FROM LOW- TO HIGH-FREQUENCY MECHANICAL NODES

### A. Theoretical Model

As schematically shown in Fig. 1(a), the hybrid system under study is comprised of two cascaded optomechanical systems, which are connected by an optical waveguide and exhibit different optomechanical couplings. Specifically, the upstream system consists of a whisper gallery mode (WGM) and a mechanical mode with resonant frequency in the megahertz range. Considering the corresponding optomechanical configurations of microsphere [23, 49, 53, 64] and microdisk [24, 50, 59, 65], the optical cavity resonant frequency can experience a significant change induced by the mechanical oscillation, thus yielding the *dispersive* optomechanical interaction. Thanks to the strong localization on the electromagnetic field in these small-sized devices, the bare optomechanical coupling can get strengthened up to sub-kilohertz [10]. Via mediation of the optical waveguide in the telecom wavelength, the optical output field from the upstream optomechanical system can transmit to the downstream one, which supports two optical WGMs, a high-frequency mechanical mode in the gigahertz range, and the phonon BLS-induced *triple-resonant* interaction [27, 28]. Actually, by resonantly driving any one cavity mode in this system, the BLS process can lead to a pronounced asymmetry between the Stokes and anti-Stokes sidebands. Hence, we can selectively activate the parametric-down conversion or beam-splitter (state transfer) interactions in this system. As a result, the Hamiltonian describing two

separated systems in Fig. 1(a) reads (in units of  $\hbar$ )

$$\begin{aligned} H &= H_f + H_{\text{int}} + H_{\text{dri}}, \\ H_f &= \omega_c c^\dagger c + \omega_b b^\dagger b + \omega_1 a_1^\dagger a_1 + \omega_2 a_2^\dagger a_2 + \omega_m m^\dagger m, \\ H_{\text{int}} &= -g_c c^\dagger c (b + b^\dagger) + g (a_1^\dagger a_2 m + a_1 a_2^\dagger m^\dagger), \\ H_{\text{dri}} &= i\epsilon (c^\dagger e^{-i\omega_l t} - c e^{i\omega_l t}) + i\epsilon_2 (a_2^\dagger e^{-i\omega_0 t} - a_2 e^{i\omega_0 t}), \end{aligned} \quad (1)$$

where  $O_l = c, b$ , ( $O_r = a_1, a_2$  and  $m$ ) and  $O_l^\dagger$  ( $O_r^\dagger$ ) represent the mode operators of the optical cavity mode and low-frequency mechanical mode (two WGMs and high-frequency mechanical mode) embodied by the upstream (downstream) optomechanical system depicted in Fig. 1(a), respectively.  $\omega_{O_l(O_r)}$  denote the corresponding resonant frequencies. The second term  $H_{\text{int}}$  involves dispersive and triple-resonant interactions between the photons and phonons in this hybrid model, with coupling strengths  $g_c$  and  $g$ . They are typically weak, but the effective coupling strengths can be greatly enhanced by adopting the corresponding drives to excite the specific physical process. In the third term,  $H'_{\text{dri}} = i\hbar\epsilon (c^\dagger e^{-i\omega_l t} - c e^{i\omega_l t})$  describes a strong red-detuned pump applied on the optical cavity, where  $\epsilon = \sqrt{\kappa_c P / \hbar \omega_l}$ , jointly determined by the cavity mode dissipation  $\kappa_c$ , the drive power  $P$  and frequency  $\omega_l$ , introduces the coupling strength between the cavity and drive fields.  $H''_{\text{dri}} = i\hbar\epsilon_2 (a_2^\dagger e^{-i\omega_0 t} - a_2 e^{i\omega_0 t})$  characterizes the drive resonant to the optical WGM  $a_2$ , with cavity decay rate  $\kappa_a$ , the driving frequency  $\omega_0$ , and power  $P_2$ .

We note that the Hamiltonian (1) is provided without considering the physical coupling between two remote optomechanical systems. Instead, the optical cavity modes in such two spatially separated microresonators can be effectively connected by an optical waveguide of telecom wavelength, thus facilitating the directional coupling that enables the propagation of the output field of upstream system  $c_{\text{out}} = \sqrt{\kappa_c} c - \tilde{c}_{\text{in}}$  [66] to the input of the downstream system but not vice versa. Here,  $\tilde{c}_{\text{in}}$  refers to both the optical drive  $\epsilon$  of cavity mode  $c$  and its input noise  $c_{\text{in}}$ . In theory, the waveguide transmission procedure can be modeled by an equivalent beam-splitter [67–70], such that the input field of optical WGM can be rewritten by

$$\tilde{a}_{1,\text{in}} = \sqrt{\eta} c_{\text{out}} + \sqrt{1-\eta} a_{1,\text{in}}, \quad (2)$$

where  $\eta$  and  $a_{1,\text{in}}$  describes the coupling efficiency and input thermal noise. As a consequence, including the dissipation and input noise of each mode and working in the rotating frame with respect to  $\hbar\omega_l (c^\dagger c + a_1^\dagger a_1) + \hbar\omega_0 a_2^\dagger a_2 + \hbar(\omega_l - \omega_0) m^\dagger m$ , we can obtain the quantum Langevin equations (QLEs) of whole model

$$\begin{aligned} \dot{c} &= -i\Delta_c c - \frac{\kappa_c}{2} c + ig_c c (b + b^\dagger) + \epsilon + \sqrt{\kappa_c} c_{\text{in}}, \\ \dot{b} &= -i\omega_b b - \frac{\gamma_b}{2} b + ig_c c^\dagger c + \sqrt{\gamma_b} b_{\text{in}}, \\ \dot{a}_1 &= -i\Delta_1 a_1 - \frac{\kappa_a}{2} a_1 - iga_2 m + \sqrt{\kappa_a} \tilde{a}_{1,\text{in}} \\ \dot{a}_2 &= -i\Delta_2 a_2 - \frac{\kappa_a}{2} a_2 - iga_1 m^\dagger + \epsilon_2 + \sqrt{\kappa_a} a_{2,\text{in}}, \\ \dot{m} &= -i\Delta_m m - \frac{\gamma_m}{2} m - iga_1 a_2^\dagger + \sqrt{\gamma_m} m_{\text{in}}, \end{aligned} \quad (3)$$

where  $\Delta_c = \omega_c - \omega_l$ ,  $\Delta_1 = \omega_1 - \omega_l$ ,  $\Delta_2 = \omega_2 - \omega_0$ ,  $\Delta_m = \omega_m - (\omega_l - \omega_0)$ , and  $\gamma_b$  ( $\gamma_m$ ) is the dissipation rate of the low (high)-frequency mechanical mode. Apart from  $a_{1,\text{in}}$  in Eq. (2),  $c_{\text{in}}$  and  $a_{2,\text{in}}$  also represent the zero-mean input noises of corresponding optical WGMs in the hybrid system. In general, these operators obey the following correlation:  $\langle k_{\text{in}}(t)k_{\text{in}}^\dagger(t') \rangle = [n_k(\omega_k) + 1]\delta(t-t') \approx \delta(t-t')$  ( $k = c, a_1$  and  $a_2$ ). As for the high-quality mechanical resonant modes, i.e.  $Q_{k'} = \omega_{k'}/\gamma_{k'} \gg 1$  ( $k' = b$  and  $m$ ), we can further take the Markovian approximation [71] to describe the autocorrelation of noises:  $\langle k'_{\text{in}}(t)k'_{\text{in}}{}^\dagger(t') \rangle = \langle k'_{\text{in}}{}^\dagger(t)k'_{\text{in}}(t') \rangle + \delta(t-t') \approx [n_{k'}(\omega_{k'}) + 1]\delta(t-t')$ , where  $n_{k'}(\omega_{k'}) = 1/[\exp(\hbar\omega_{k'}/k_B T) - 1]$  is the mean thermal excitation number of the specific mechanical mode at temperature  $T$ , with Boltzman constant  $k_B$ .

## B. Linearization and Covariance Matrix

In cavity optomechanics, a prerequisite to establish quantum entanglement is to enhance the nonlinear optomechanical interaction. To achieve this, we adopt to simultaneously

$$A = \begin{pmatrix} -\frac{\kappa_c}{2} & \tilde{\Delta}_c & -2\text{Im}G_c & 0 & 0 & 0 & 0 & 0 & 0 & 0 & 0 \\ -\tilde{\Delta}_c & -\frac{\kappa_c}{2} & 2\text{Re}G_c & 0 & 0 & 0 & 0 & 0 & 0 & 0 & 0 \\ 0 & 0 & -\frac{\gamma_b}{2} & \omega_b & 0 & 0 & 0 & 0 & 0 & 0 & 0 \\ 2\text{Re}G_c & 2\text{Im}G_c & -\omega_b & -\frac{\gamma_b}{2} & 0 & 0 & 0 & 0 & 0 & 0 & 0 \\ \sqrt{\kappa_a\kappa_c\eta} & 0 & 0 & 0 & -\frac{\kappa_a}{2} & \Delta_1 & \text{Im}G_m & \text{Re}G_m & \text{Im}G_2 & \text{Re}G_2 & \\ 0 & \sqrt{\kappa_a\kappa_c\eta} & 0 & 0 & -\Delta_1 & -\frac{\kappa_a}{2} & -\text{Re}G_m & \text{Im}G_m & -\text{Re}G_2 & \text{Im}G_2 & \\ 0 & 0 & 0 & 0 & -\text{Im}G_m & \text{Re}G_m & -\frac{\kappa_a}{2} & \Delta_2 & \text{Im}G_1 & -\text{Re}G_1 & \\ 0 & 0 & 0 & 0 & -\text{Re}G_m & -\text{Im}G_m & -\Delta_2 & -\frac{\kappa_a}{2} & -\text{Re}G_1 & -\text{Im}G_1 & \\ 0 & 0 & 0 & 0 & -\text{Im}G_2 & \text{Re}G_2 & \text{Im}G_1 & -\text{Re}G_1 & -\frac{\gamma_m}{2} & \Delta_m & \\ 0 & 0 & 0 & 0 & -\text{Re}G_2 & -\text{Im}G_2 & -\text{Re}G_1 & -\text{Im}G_1 & -\Delta_m & -\frac{\gamma_m}{2} \end{pmatrix}, \quad (5)$$

where  $G_c = g_c\langle c \rangle$ ,  $G_1 = g\langle a_1 \rangle$ ,  $G_2 = g\langle a_2 \rangle$  and  $G_m = g\langle m \rangle$  are the effective coupling strengths established by the strong pumps in this scheme, and  $\langle c \rangle$ ,  $\langle a_1 \rangle$ ,  $\langle a_2 \rangle$  and  $\langle m \rangle$  denote the corresponding steady-state excitations, which can be directly derived from the expanded equations for steady-state average:

$$\begin{aligned} 0 &= -i\tilde{\Delta}_c\langle c \rangle - \frac{\kappa_c}{2}\langle c \rangle + \epsilon, \\ 0 &= -i\Delta_1\langle a_1 \rangle - \frac{\kappa_a}{2}\langle a_1 \rangle - ig\langle a_2 \rangle\langle m \rangle + \sqrt{\kappa_a\kappa_c\eta}\langle c \rangle - \sqrt{\kappa_a}\langle c_{\text{in}} \rangle \\ &= -i\Delta_1\langle a_1 \rangle - \frac{\kappa_a}{2}\langle a_1 \rangle - ig\langle a_2 \rangle\langle m \rangle + \sqrt{\kappa_a\kappa_c\eta}\langle c \rangle - \sqrt{\kappa_a}\kappa_c\epsilon, \\ 0 &= -i\Delta_2\langle a_2 \rangle - \frac{\kappa_a}{2}\langle a_2 \rangle - ig\langle a_1 \rangle\langle m \rangle^* + \epsilon_2, \\ 0 &= -i\Delta_1\langle m \rangle - \frac{\gamma_m}{2}\langle m \rangle - ig\langle a_1 \rangle\langle a_2 \rangle^*. \end{aligned} \quad (6)$$

Besides, in Eqs. (5) and (6),  $\tilde{\Delta}_c = \Delta_c - g_c\langle c \rangle(\langle b \rangle + \langle b \rangle^*)$  is the effective detuning of the WGM  $a_1$  with respect to the optical drive at  $\omega_l$ , which includes the optical resonant frequency change under the dispersive optomechanical interaction.

pump the optical modes  $c$  and  $a_2$ . Via the mediation of optical waveguide, the optical WGM  $a_1$  can also attain a strong activation, which leads to  $|\langle c \rangle|$ ,  $|\langle a_1 \rangle|$  and  $|\langle a_2 \rangle| \gg 1$ . Therefore, when the system evolves into the steady state after a sufficient period, we can study the system dynamics by expanding each mode operator as the sum of its steady-state average and the quantum fluctuations:  $O_i = \langle O_i \rangle + \delta O_i$  ( $i \in \{l, r\}$ ), which enables us to obtain the linearized QLEs about the quantum fluctuation terms of all modes in the hybrid system. Following the definitions of quantum quadratures  $\delta X_{O_i} = (\delta O_i + \delta O_i^\dagger)/\sqrt{2}$ ,  $\delta Y_{O_i} = -i(\delta O_i - \delta O_i^\dagger)/\sqrt{2}$ , the linearized QLEs can be further rewritten as a time-dependent differential equation of the quadrature vector  $u(t) = \{\delta X_c(t), \delta Y_c(t), \delta X_b(t), \delta Y_b(t), \delta X_{a_1}(t), \delta Y_{a_1}(t), \delta X_{a_2}(t), \delta Y_{a_2}(t), \delta X_m(t), \delta Y_m(t)\}^T$ :

$$\dot{u}(t) = Au(t) + n(t), \quad (4)$$

where  $n(t) = \{\sqrt{\kappa_c}X_{c,\text{in}}(t), \sqrt{\kappa_c}Y_{c,\text{in}}(t), \sqrt{\gamma_b}X_{b,\text{in}}(t), \sqrt{\gamma_b}Y_{b,\text{in}}(t), \sqrt{\kappa_a}X_{\bar{a}_1,\text{in}}(t), \sqrt{\kappa_a}Y_{\bar{a}_1,\text{in}}(t), \sqrt{\kappa_a}X_{a_2,\text{in}}(t), \sqrt{\kappa_a}Y_{a_2,\text{in}}(t), \sqrt{\gamma_m}X_{m,\text{in}}(t), \sqrt{\gamma_m}Y_{m,\text{in}}(t)\}^T$  represents the vector of the input noises, among which  $\bar{a}_{1,\text{in}} = \sqrt{1 - \eta}a_{1,\text{in}} - \sqrt{\eta}c_{\text{in}}$ . More importantly, the drift matrix is provided as

Considering the gaussian nature of all input noises in this system, it can be anticipated that the quantum dynamics governed by the linearized QLEs (4) will finally evolve into the gaussian state, which can be characterized by a  $10 \times 10$  covariance matrix (CM), with each element defined by  $V_{ij} = \langle u_i(t)u_j(t') + u_j(t')u_i(t) \rangle / 2$  ( $i, j \in \{1, 2, \dots, 10\}$ ). Specifically, the steady-state CM can be obtained by solving the so-called Lyapunov equation [72]

$$AV + VA^T + D = 0. \quad (7)$$

It is obvious that except drift matrix  $A$ , the steady-state CM  $V$  also depends on the diffusion matrix  $D$  which denotes the corresponding CM of different noises in vector  $n(t)$ . With each entry defined by  $D_{ij}\delta(t-t') = \langle n_i(t)n_j(t') + n_j(t')n_i(t) \rangle / 2$ , it takes the form of

$$D = \begin{pmatrix} D_c & 0 & D_{ca_1} \\ 0 & D_b & 0 \\ D_{ca_1} & 0 & D_{a_1} \end{pmatrix} \oplus \begin{pmatrix} D_{a_2} & 0 \\ 0 & D_m \end{pmatrix}, \quad (8)$$

where  $D_c = \kappa_c(n_c + 1/2)I_2$ ,  $D_b = \gamma_b(n_b + 1/2)I_2$ ,  $D_{a_1} = \kappa_a[(1 - \eta)(n_c + 1/2) + \eta(n_{a_1} + 1/2)]I_2$ ,  $D_{a_2} = \kappa_a(n_{a_2} + 1/2)I_2$ ,

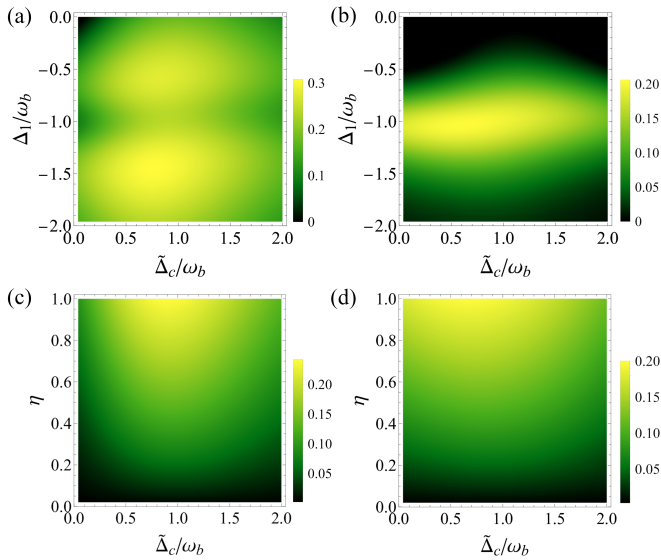


FIG. 2. Density plot of steady-state (a)  $E_{a_1 b}$  and (b)  $E_{m b}$  versus the detunings  $\tilde{\Delta}_c$  and  $\Delta_1$ ; (c)  $E_{a_1 b}$  and (d)  $E_{m b}$  versus the detuning  $\tilde{\Delta}_c$  and the coupling efficiency  $\eta$ . Note that we take  $\eta = 1$  in (a) and (b), and  $\Delta_1/\omega_b = -1$  in (c) and (d). See main text for other plotting parameters.

$D_m = \gamma_m(n_m + 1/2)I_2$ , including  $2 \times 2$  identity matrix  $I_2$ . Moreover, the off-diagonal part  $D_{ca_1} = -\sqrt{\kappa_a \kappa_c \eta}(n_c + 1/2)I_2$  features the correlation between input noises of  $c_{in}$  and  $\tilde{a}_{1,in} = \sqrt{1 - \eta}a_{1,in} - \sqrt{\eta}c_{in}$ .

### C. Results and Discussion

Here, based on this hybrid system, we provide an accessible scheme to realize quantum entanglement of two distant mechanical nodes with resonant frequencies in completely different frequency ranges. As depicted in Fig. 1(b), we adopt the mechanism to redistribute the quantum entanglement generated in the upstream system including low-frequency mechanical mode to the downstream system with a high-frequency mechanical resonance in the network. In this hybrid model, the mechanical mode supported by the upstream optomechanical system owns the megahertz resonant frequency, and takes high thermal population even at cryogenic temperatures, which inhibits the generation of quantum entanglement. To overcome this, following the pioneering works [72–74], we apply a *sufficiently strong red-detuned* optical drive field to cool the mechanical mode and simultaneously entangle it with the cavity mode  $c$ , shown by the inset (1) in Fig. 1(a). Specifically, such a strong drive enables to yield an enhanced optomechanical coupling  $G_c$ , which can not only strengthen the optomechanical anti-Stokes scattering and activate the beam-splitter interaction  $H_{as} \propto bc^\dagger + b^\dagger c$  to greatly reduce the mechanical thermal effect, but also highlight the role played by the Stokes scattering to stimulate parametric-down conversion interaction  $H_S \propto bc + b^\dagger c^\dagger$ , owing to that the strong optomechanical coupling  $G_c$  breaks the

weak-coupling condition  $G_c \ll \omega_b$  to take the rotating-wave approximation (RWA) in the general red-detuned driving case [10, 72, 75, 76]. Therefore, the optical cavity output field transmitted to the downstream optomechanical system can be filtered by the corresponding optical cavity with WGM  $a_1$  resonant to the optical down-conversion sideband component which exhibits the most significant entanglement with the low-frequency mechanical mode  $b$ . The established quantum correlation can be further distributed to the downstream optomechanical system embodying the high-frequency mechanical node. To achieve this, we choose to utilize the approach manifested in inset (2) of Fig. 1(a). Correspondingly, the optical WGM  $a_2$  is pumped by a resonant drive ( $\Delta_2 = 0$  and thus  $\Delta_m = \omega_m + \omega_0 - \omega_l = \omega_1 - \omega_l = \Delta_1$ ), which can effectively activate the optomechanical state-transfer interaction between the optical WGM  $a_1$  and the gigahertz mechanical mode  $m$ . As a result, the quantum entanglement carried by the output field of the left optomechanical subsystem in Fig. 1(a) can be further distributed to the high-frequency mechanical node, hence realizing the remote macroscopic entanglement between two types of distinct mechanical systems with a far-detuned resonant frequency mismatch.

To quantify bipartite entanglement in the hybrid system, we consider the logarithmic negativity  $E_N$  [72, 77] as the quantum measure, which can be obtained from the CM of any two-mode subsystem. In Fig. 2(a) (Fig. 2(b)), we show the bipartite entanglement  $E_{a_1 b}$  ( $E_{m b}$ ) versus the detunings  $\tilde{\Delta}_c$  and  $\Delta_1$ , by employing experimentally feasible parameters [10, 27, 28, 64]:  $\omega_b/2\pi = 10$  MHz,  $\omega_m/2\pi = 8.2$  GHz,  $\lambda_c = \lambda_{a_1} \approx \lambda_{a_2} \approx 1550$  nm,  $\kappa_c = \kappa_a = 2.0 \omega_b$ ,  $\gamma_b = 10^{-4} \omega_b$ ,  $\gamma_m = 0.5 \omega_b$ ,  $g_c/2\pi = 10^2$  Hz,  $g/2\pi = 20$  Hz,  $\eta = 1$ ,  $T = 10$  mK. Besides, in plotting Figs. 1(a) and 1(b), we mainly study the quantum entanglement established under fixed coupling strengths:  $|G_c|/2\pi = |G_2|/2\pi = 3.0$  MHz, which can be achieved via the specific optical drivings  $\epsilon$  and  $\epsilon_2$  at different detunings  $\tilde{\Delta}_c$  and  $\Delta_1$  (see Eq. (6) about the steady-state excitations). Meanwhile, the coupling strengths  $G_1$  and  $G_m$  can also be correspondingly determined. Clearly, exploiting the strong red-detuned pump  $\tilde{\Delta}_c \approx \omega_b$ , the steady-state entanglement  $E_{a_1 b}$  and  $E_{m b}$  significantly emerge near the down-conversion sideband ( $\omega_l \approx \omega_1 - \omega_b$ ), which confirms the entanglement mechanism we discussed above. Another typical sign in these two subfigures is the complementary entanglement distribution between them. It reflects that the entanglement behaves like a finite quantum resource. Figs. 2(c) and 2(d) respectively show  $E_{a_1 b}$  and  $E_{m b}$  along with the variation of coupling efficiency  $\eta$ . The results validates our protocol in remote preparation of mechanical entanglement. Here, we note that all results presented in this section are obtained in the steady state and guaranteed by the negative eigenvalues (real parts) of the drift matrix  $A$  and its submatrixes of two optomechanical systems.

We also discuss the influence of thermal effect to our entanglement scheme. In Figs. 3(a)-3(c), we plot the steady-state entanglement  $E_{cb}$ ,  $E_{a_1 b}$  and  $E_{m b}$  established via this scheme when the optomechanical systems are respectively placed in the environment with temperature  $T_1$  and  $T_2$ . Obviously, we find that  $E_{cb}$  remains robust against the change of  $T_2$  attributed

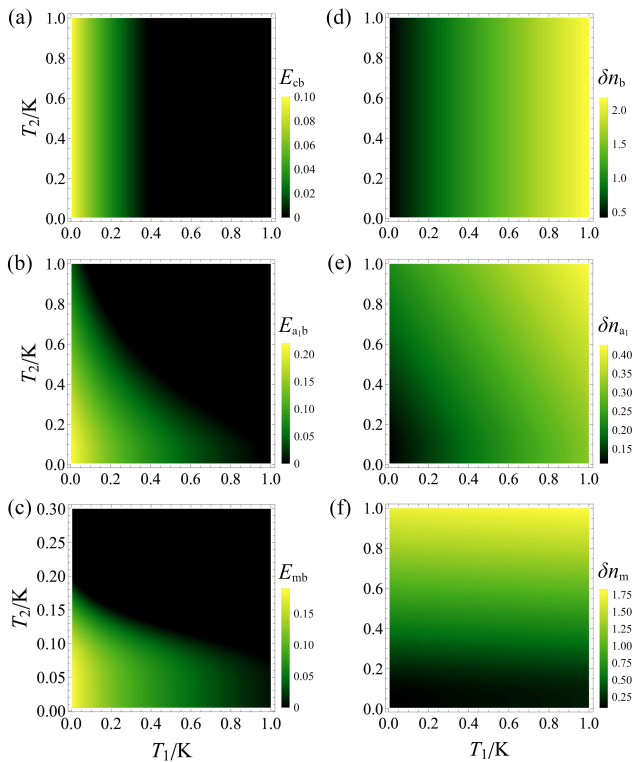


FIG. 3. Density plot of bipartite entanglement (a)  $E_{cb}$ , (b)  $E_{a_1b}$  and (c)  $E_{mb}$ ; and quantum excitations (d)  $\delta n_b$ , (e)  $\delta n_{a_1}$  and (f)  $\delta n_m$  versus the environmental temperatures  $T_1$  and  $T_2$ . Note that here we take  $\eta = 0.9$ ,  $\tilde{\Delta}_c/\omega_b = 0.75$ , and  $\Delta_1/\omega_b = -1$ . The other parameters are the same as those used in Fig. 2.

to the unidirectional coupling between the cavity modes  $c$  and  $a_1$ . In contrast,  $E_{a_1b}$  and  $E_{mb}$  are more sensitive to the variation of  $T_2$  (even surpass the influence of  $T_1$  in Fig. 3(c)). This might be a bit of counter-intuitive because that the megahertz mechanical mode usually experiences more thermal noise than the high-frequency one in the gigahertz range, thus the quantum entanglement should exist more robust to the varying of  $T_2$ . Actually, this can be explained when we analyze the intrinsic quantum excitations  $\delta n_i = (\langle \delta X_i^2 \rangle + \langle \delta Y_i^2 \rangle - 1)/2$  ( $i = b, a_1$  and  $m$ ) embodied in the quantum quadratures variances of each mode in the steady state (see Figs. 3(d)-3(f)). As expressed by Fig. 1(b), the quantum dynamics of  $a_1$  is not only affected by the output field of cavity mode  $c$  which brings the nonlocal quantum entanglement and thus can be equivalently recognized as an external quantum reservoir, but also influenced by the thermal noise from the mechanical mode  $m$ . Once the temperature  $T_2$  increases, the thermal effect of  $m$  becomes more remarkable. However, not as the upstream optomechanical system with effective cooling mechanism activated by the strong red-detuned pump, in the downstream optomechanical system the cooling mechanism is absent, and the mechanical thermal effect tends to dissipate into the physical systems (optical WGMs) with larger dissipation rates, as in Fig. 3(e), which gives rise to entanglement dependence on  $T_2$ . For high-frequency mechanical node  $m$ , the thermal noise arising from increasing  $T_2$  is more significant than that from

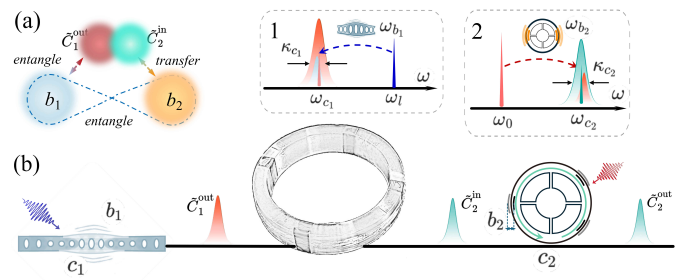


FIG. 4. Schematic diagrams of the (a) physical mechanism and (b) hybrid system to realize the remote gigahertz-to-megahertz mechanical entanglement distribution. Inset 1: Entanglement preparation process. A blue-detuned optical pulse is used to activate the quantum entanglement between the optical output temporal mode ( $C_1^{\text{out}}$ ) and the gigahertz mechanical node ( $b_1$ ). Inset 2: Entanglement distribution process. After the long-distance propagation in optical waveguide, the quantum entanglement can be further distributed to megahertz mechanical node ( $b_2$ ) via the beam-splitter interaction activated by the red-detuned pulse.

$T_1$  (see Fig. 3(f)). As a result, the mechanical entanglement  $E_{mb}$  is more insensitive to the variation of  $T_1$  than  $T_2$ .

### III. REMOTE ENTANGLEMENT DISTRIBUTION FROM HIGH- TO LOW-FREQUENCY MECHANICAL NODES

In the last section, we have introduced a protocol to achieve the macroscopic entanglement of two mechanical nodes by transmitting the optical field which brings the quantum entanglement with the megahertz mechanical mode to the remote optomechanical system supporting gigahertz mechanical mode. On the other hand, how to achieve the quantum entanglement redistribution from the high- to low-frequency mechanical nodes is also worthy of study. Specifically, the scheme we proposed in last section is not subject to this case, owing to that: for the protocol we discussed in Fig. 1(a), because of the absence of cooling mechanism, the thermal effect exhibited by mechanical node in the downstream optomechanical system needs to be strictly restricted. However, under the condition that the mechanical resonant frequency lies in the megahertz range, the mechanical thermal effect can act to prevent the establishment of the distant mechanical entanglement even in the cryogenic temperature.

#### A. Theoretical Proposal

We proceed a new approach to achieve entanglement distribution from the high-frequency mechanical node to the remote low-frequency one, by exploiting the fast optical pulses with optomechanical system [11, 43]. In this scheme, we consider a hybrid model which is comprised of two optomechanical systems linked by a long-distance optical waveguide. As shown in Fig. 4, the upstream system, e.g. the optomechanical crystal [10–14, 19, 43], supports the mechanical mode with resonant frequency in the gigahertz range

and holds nonlinear dispersive coupling. Its Hamiltonian consists of three terms  $H' = H'_0 + H'_{\text{int}} + H'_{\text{dri+}}$ , including free Hamiltonian  $H'_0 = \hbar\omega_{c_1}c_1^\dagger c_1 + \hbar\omega_{b_1}b_1^\dagger b_1$ , interaction  $H'_{\text{int}} = -\hbar g_1 c_1^\dagger c_1 (b_1 + b_1^\dagger)$ , and driving  $H'_{\text{dri+}} = i\hbar\epsilon'(c_1^\dagger e^{-i\omega t} - c_1 e^{i\omega t})$ . This presents a ideal platform to prepare the optomechanical entangled state using nonlinear coupling. Therefore, we choose to enhance the optomechanical Stokes scattering by sending a blue-detuned optical pulse ( $\omega_l = \omega_{c_1} + \omega_{b_1}$ ) to the upstream optomechanical system. In resolved sideband regime, this can activate a parametric-down conversion interaction  $H_b = -\hbar G_b (b_1 c_1 + b_1^\dagger c_1^\dagger)$  between the cavity photons and the gigahertz mechanical phonons, which dominates the dynamics of the optomechanical system during the pulse operation and leads to following QLEs in the interaction picture:

$$\begin{aligned} \dot{c}_1 &= iG_b b_1^\dagger - \frac{\kappa_{c_1}}{2} c_1 + \sqrt{\kappa_c} c_1^{\text{in}}, \\ \dot{b}_1 &\approx iG_b c_1^\dagger. \end{aligned} \quad (9)$$

Specifically, we considered a *weak* flat-top pulse with duration much shorter than the mechanical lifetime, thus the dissipation of mechanical mode can be regarded to be negligibly small and we can safely neglect it to simplify the model. Given by weak coupling  $G_b \ll \kappa_{c_1}$ , the dynamics of the cavity mode can be adiabatically eliminated to obtain  $c_1 \approx 2/\kappa_{c_1} (iG_b b_1^\dagger + \sqrt{\kappa_c} c_1^{\text{in}})$ . Accounting for the cavity input-output relation:  $c_1^{\text{out}} = \sqrt{\kappa_{c_1}} c_1 - c_1^{\text{in}}$  [66], we can obtain

$$\begin{aligned} c_1^{\text{out}} &= i\sqrt{2\mathcal{G}_b} b_1^\dagger + c_1^{\text{in}}, \\ \dot{b}_1 &= -\mathcal{G}_b b_1 + i\sqrt{2\mathcal{G}_b} c_1^{\text{out}}, \end{aligned} \quad (10)$$

where  $\mathcal{G}_b = 2G_b^2/\kappa_{c_1}$ . Following the pioneering studies in cavity optomechanics [78, 79] and related cavity magnonics [69, 80], we can describe the physical process of entanglement preparation via defining a set of normalized temporal modes for the cavity mode driven by a pulse with duration  $\tau_b$ , which gives that

$$\tilde{C}_1^{\text{in}}(\tau_b) = \sqrt{\frac{2\mathcal{G}_b}{1 - e^{-2\mathcal{G}_b\tau_b}}} \int_0^{\tau_b} e^{-\mathcal{G}_b s} c_1^{\text{in}}(s) ds, \quad (11a)$$

$$\tilde{C}_1^{\text{out}}(\tau_b) = \sqrt{\frac{2\mathcal{G}_b}{e^{2\mathcal{G}_b\tau_b} - 1}} \int_0^{\tau_b} e^{\mathcal{G}_b s} c_1^{\text{out}}(s) ds. \quad (11b)$$

Equipped with the necessary tool (11), we can integrate (10) to get:

$$\begin{aligned} \tilde{C}_1^{\text{out}}(\tau_b) &= i\sqrt{e^{2\mathcal{G}_b\tau_b} - 1} b_1^\dagger(0) + e^{\mathcal{G}_b\tau_b} \tilde{C}_1^{\text{in}}(\tau_b), \\ b_1(\tau_b) &= e^{\mathcal{G}_b\tau_b} b_1(0) + i\sqrt{e^{2\mathcal{G}_b\tau_b} - 1} \tilde{C}_1^{\text{in}}(\tau_b), \end{aligned} \quad (12)$$

and extract the corresponding propagator [79]

$$U_b(\tau_b) = e^{i\text{tanh}r \tilde{C}_1^{\text{in}\dagger} b_1^\dagger} \text{cosh}r^{-1} \tilde{C}_1^{\text{in}\dagger} \tilde{C}_1^{\text{in}} - b_1^\dagger b_1 e^{-i\text{tanh}r \tilde{C}_1^{\text{in}} b_1}, \quad (13)$$

which allows the effective transformations from  $b(0)$  and  $\tilde{C}_1^{\text{in}}(0)$  to  $b(\tau_b) = U_b^\dagger(\tau_b) b(0) U_b(\tau_b)$  and  $\tilde{C}_1^{\text{out}}(\tau_b) = U_b^\dagger(\tau_b) \tilde{C}_1^{\text{in}}(\tau_b) U_b(\tau_b)$ . Here, we simplified the expression by  $\text{cosh}r = e^{\mathcal{G}_b\tau_b}$ ,  $\text{tanh}r = \sqrt{1 - e^{-2\mathcal{G}_b\tau_b}}$ , both of which includes the squeezed

parameter  $r$  characterizing the parametric-down conversion-related squeezing strength.

Considering  $\rho_{b_1}(0)$  to be the initial state of low-frequency mechanical mode, the state of the upstream optomechanical system, at end of the blue-detuned optical pulse, can be represented by  $\rho_{\tilde{C}_1 b_1}(\tau) = U_b(\tau) \rho_{\tilde{C}_1 b_1}(0) U_b^\dagger(\tau) = U_b(\tau) [|0\rangle_{\tilde{C}_1} \langle 0| \otimes \rho_{b_1}(0)] U_b^\dagger(\tau)$ . To achieve the quantum entanglement, we assume that the gigahertz mechanical mode is precooled to its ground state, i.e. the mechanical initial state  $\rho_{b_1}(0) = |0\rangle_{b_1} \langle 0|$ , which has been successfully demonstrated in the experimental platform based on the optomechanical crystal [19, 81]. Therefore, after a pulse period of  $\tau_b$ , the quantum state

$$\begin{aligned} \rho_{\tilde{C}_1 b_1}(\tau_b) &= \\ &(\text{cosh}r)^{-2} \sum_{n=0}^{\infty} \sum_{n'=0}^{\infty} (i\text{tanh}r)^n |n, n\rangle_{\tilde{C}_1 b_1} \langle n', n'| (-i\text{tanh}r)^{n'} \end{aligned} \quad (14)$$

is a two-mode squeezed vacuum state referring to the high-frequency mechanical mode and the optical output temporal mode. Such state, intrinsically embodying the nature of quantum entanglement, can be characterized by the quantum measure of logarithmic negativity  $E_N = 2r$ .

As illustrated by the sketch in Fig. 4, with the mediation of the optical waveguide, the output temporal pulse can propagate towards the downstream optomechanical system, which holds the low-frequency mechanical mode in the megahertz range. In order to realize the entanglement distribution onto the low-frequency mechanical node, this system is driven by a red-detuned optical pulse to excite the beam-splitter interaction  $H_r = -\hbar G_r (b_1 c_1^\dagger + b_1^\dagger c_1)$ . In this context, we mainly consider the optomechanical configuration of microresonators [10] and assume that the duration of used fast optical pulse is much smaller than the coherent lifetime of the mechanical mode  $\tau_r \ll 1/\gamma_b$ . Therefore, we can safely exclude the dissipation-related terms in the QLEs and simplify the model by adiabatically eliminated the optical cavity mode  $c_2$  to get  $c_2 \approx 2/\kappa_{c_2} (iG_r b_2 + \sqrt{\kappa_{c_2}} c_2^{\text{in}})$ . Similar to (10) in the entanglement generation process, we can obtain

$$\begin{aligned} c_2^{\text{out}} &= i\sqrt{2\mathcal{G}_r} b_2 + c_2^{\text{in}}, \\ \dot{b}_2 &= \mathcal{G}_r b_2 + i\sqrt{2\mathcal{G}_r} c_2^{\text{out}}, \end{aligned} \quad (15)$$

by combining the cavity input-output relation  $c_2^{\text{out}} = \sqrt{\kappa_{c_2}} c_2 - c_2^{\text{in}}$ , with  $\mathcal{G}_r = 2G_r^2/\kappa_{c_2}$ . Following the integration process to get (12), this achieve a beam-splitter type  $2 \times 2$  unitary transformation

$$\begin{aligned} \tilde{C}_2^{\text{out}}(\tau_r) &= i\sqrt{1 - e^{-2\mathcal{G}_r\tau_r}} b_2(0) + e^{-\mathcal{G}_r\tau_r} \tilde{C}_2^{\text{in}}(\tau_r), \\ b_2(\tau_r) &= e^{-\mathcal{G}_r\tau_r} b_2(0) + i\sqrt{1 - e^{-2\mathcal{G}_r\tau_r}} \tilde{C}_2^{\text{in}}(\tau_r), \end{aligned} \quad (16)$$

by defining of a set of normalized temporal modes

$$\tilde{C}_2^{\text{in}}(\tau_r) = \sqrt{\frac{2\mathcal{G}_r}{e^{2\mathcal{G}_r\tau_r} - 1}} \int_0^{\tau_r} e^{\mathcal{G}_r s'} c_2^{\text{in}}(s') ds', \quad (17a)$$

$$\tilde{C}_2^{\text{out}}(\tau_r) = \sqrt{\frac{2\mathcal{G}_r}{1 - e^{-2\mathcal{G}_r\tau_r}}} \int_0^{\tau_r} e^{-\mathcal{G}_r s'} c_2^{\text{out}}(s') ds'. \quad (17b)$$

Briefly introduced the entanglement proposal sketched in Fig. 4(a), afterwards we can specifically discuss the quantum state in subsequent process of entanglement distribution.

## B. Entanglement Redistribution

For building a long-distance quantum network which connects two distinct mechanical nodes via the optical mediation, the transmission loss is practically unavoidable. The optical loss significantly increases along with the transmission distance, therefore it can be theoretically described by the linear beam-splitter model [67–69], where  $R$  and  $T$  respectively represent the reflectance and transmittance of the beam-splitter and satisfy  $R + T = 1$ . Naturally, this transformation provides a clear relation about the output temporal mode  $\tilde{C}_1^{\text{out}}$  and the input temporal mode  $\tilde{C}_2^{\text{in}}$  (see Fig. 5). With the bridge of it, we can turn into the quantum state after a transmitting time of  $\Delta\tau$ :

$$\begin{aligned} \rho_{\tilde{C}_2 b_1}(\tau_b + \Delta\tau) = & (\cosh r)^{-2} \sum_{n=0}^{\infty} \sum_{n'=0}^{\infty} (i \tanh r)^n (-i \tanh r)^{n'} |n\rangle_{b_1} \langle n'| \otimes \\ & \sum_{t=0}^{\min(n, n')} \sqrt{\frac{n! n'!}{(t!)^2 (n-t)! (n'-t)!}} R^t T^{\frac{n+n'}{2}-t} |n-t\rangle_{\tilde{C}_2^{\text{out}}} \langle n'-t|, \end{aligned} \quad (18)$$

Expressed by (16), the pulse-assisted state transfer process introduces the output temporal mode  $\tilde{C}_2^{\text{out}}$  and low-frequency mechanical mode  $b_2$  which is assumed to be precooled to its ground state [23, 24, 50, 82]. The initial state, before activating the optomechanical beam-splitter interaction in the down-

stream optomechanical system, can arrive at

$$\rho_{\text{BS}}(0) = \rho_{\tilde{C}_2 b_1}(\tau_b + \Delta\tau) \otimes |0, 0\rangle_{\tilde{C}_2^{\text{out}} b_2} \langle 0, 0|. \quad (19)$$

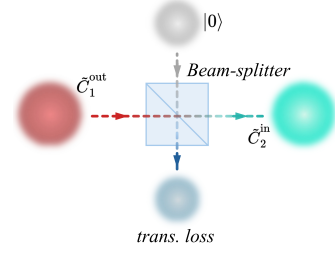


FIG. 5. Sketch of the transmission loss model.

As a result, the transformation (16) enables us to obtain the quantum state after a red-detuned pulse of  $\tau_r$

$$\begin{aligned} \rho_{\text{BS}}(\tau_r) = & (\cosh r)^{-2} \sum_{n=0}^{\infty} \sum_{n'=0}^{\infty} (i \tanh r)^n (-i \tanh r)^{n'} |n\rangle_{b_1} \langle n'| \\ & \otimes \sum_{t=0}^{\min(n, n')} \sqrt{\frac{n! n'!}{(t!)^2 (n-t)! (n'-t)!}} R^t T^{\frac{n+n'}{2}-t} \\ & \sum_{q=0}^{n-t} \sum_{p=0}^{n'-t} \sqrt{\frac{(n-t)! (n'-t)!}{q! p! (n-t-q)! (n'-t-p)!}} \\ & i^q (-i)^p W^{\frac{p+q}{2}} (1-W)^{\frac{n+n'-p-q}{2}-t} |q\rangle_{b_2} \langle p| \\ & \otimes |n-t-q\rangle_{\tilde{C}_2^{\text{out}}} \langle n'-t-p| \otimes |0\rangle_{\tilde{C}_2^{\text{in}}} \langle 0|, \end{aligned} \quad (20)$$

with the optomechanical state transfer efficiency  $W = 1 - e^{-2g_r \tau_r}$ . By tracing out unrelated modes, we can extract the density matrix which characterizes the subsystem of two mechanical nodes in this network:

$$\begin{aligned} \rho_{\text{sub}} = \rho_{b_1 b_2} & = \text{Tr}_{\tilde{C}_2} [\rho_{\text{BS}}(\tau_r)] \\ & = (\cosh r)^{-2} \sum_{n=0}^{\infty} \sum_{n'=0}^{\infty} (i \tanh r)^n (-i \tanh r)^{n'} |n\rangle_{b_1} \langle n'| \otimes \sum_{t=0}^{\min(n, n')} \sqrt{\frac{n! n'!}{(t!)^2 (n-t)! (n'-t)!}} R^t T^{\frac{n+n'}{2}-t} \\ & \sum_{l=0}^{\min(n-t, n'-t)} \sqrt{\frac{(n-t)! (n'-t)!}{(l!)^2 (n-t-l)! (n'-t-l)!}} i^{n-t-l} (-i)^{n'-t-l} W^{\frac{n+n'-t-l}{2}-l} (1-W)^l |n-t-l\rangle_{b_2} \langle n'-t-l|, \end{aligned} \quad (21)$$

from which we can successfully derive the CM corresponding to this two-mode state. Using the CM definition  $V_{ij} = \frac{1}{2} \langle \xi_i \xi_j + \xi_j \xi_i \rangle - \langle \xi_i \rangle \langle \xi_j \rangle = \frac{1}{2} [\text{Tr}(\rho_{\text{sub}} \xi_i \xi_j) + \text{Tr}(\rho_{\text{sub}} \xi_j \xi_i)] - \text{Tr}(\rho_{\text{sub}} \xi_i) \times \text{Tr}(\rho_{\text{sub}} \xi_j)$ , where  $i, j \in \{1, 2, 3, 4\}$  and  $\xi = \{\delta X_{b_1}, \delta Y_{b_1}, \delta X_{b_2},$

$\delta Y_{b_2}\}^T$ , the calculated CM reads

$$V_{\text{sub}} = \begin{pmatrix} \frac{1}{2} \cosh 2r & 0 & -\frac{\sqrt{WT}}{2} \sinh 2r & 0 \\ 0 & \frac{1}{2} \cosh 2r & 0 & \frac{\sqrt{WT}}{2} \sinh 2r \\ -\frac{\sqrt{WT}}{2} \sinh 2r & 0 & WT \sinh^2 r + \frac{1}{2} & 0 \\ 0 & \frac{\sqrt{WT}}{2} \sinh 2r & 0 & WT \sinh^2 r + \frac{1}{2} \end{pmatrix}.$$

(22)

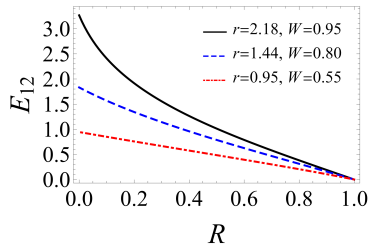


FIG. 6. The macroscopic entanglement  $E_{12}$  versus the reflectivity (optical loss)  $R$  under different conditions, with two-mode squeezing and state conversion parameters:  $r = 2.18$  and  $W = 0.95$  (solid),  $r = 1.44$  and  $W = 0.80$  (dashed), and  $r = 0.95$  and  $W = 0.55$  (dot-dashed).

Following section II, we adopt the quantum measure logarithmic negativity  $E_{12}$  to characterize the macroscopic entanglement. In Fig. 6, we show the varying of entanglement  $E_{12}$  versus the optical loss  $R$  under different two-mode squeezing and state conversion parameters, respectively, which reveals the restriction of transmission distance (considering fiber loss 0.2 dB/km at the telecom wavelength [69]) on achieved entanglement between two mechanical nodes.

Furthermore, we provide a brief discussion on the experimental feasibility of present entanglement scheme. In plotting Fig. 6, the optomechanical system with high-frequency mechanical mode, such as optomechanical crystal [11], holds telecom wavelength optical mode  $\lambda_{c_1} \approx 1550$  nm, mechanical mode resonance  $\omega_{b_1}/2\pi = 5.3$  GHz, the optical decay rate  $\kappa_{c_1}/2\pi = 1.3$  GHz  $\gg \gamma_{b_1}/2\pi$ , and supports the optomechanical coupling strength up to  $g_1/2\pi = 825$  kHz. In entanglement generation process shown in Fig. 4(b), we manage to take a blue-detuned pulse with  $\tau_b = 10$   $\mu$ s and  $P' \approx 0.4$   $\mu$ W to realize the effective optomechanical coupling  $G_1/2\pi \approx 3.93$  MHz, which gives rise to the two-mode squeezing parameter  $r \approx 2.18$ . On the other hand, for the entanglement redistribution process depicted by the inset (2) in Fig. 4(b), we mainly suggest the optomechanical microresonators as provided in Refs. [10, 82], which allow: the optical resonance near 1550 nm, the mechanical mode  $\omega_{b_2}/2\pi \approx 10^2$  MHz, optical dissipation  $\kappa_{c_2}/2\pi = 20$  MHz  $\gg \gamma_{b_2}/2\pi$ , and  $g_2/2\pi = 1.7$  kHz. By employing a red-detuned optical pulse with  $\tau_r = 10$   $\mu$ s and  $P'' \approx 33.5$   $\mu$ W, the optomechanical coupling  $G_2$  can be greatly enhanced and proceed the optomechanical state trans-

fer efficiency to  $W = 1 - e^{-2\mathcal{G}_r\tau_r} \approx 0.95$ . These analyses reflect the solidity of our theoretical scheme. Moreover, the mechanical modes supported by these two kinds of optomechanical platforms have been successfully cooled to (near) their ground states [19, 82], which also highlights feasibility of this proposal.

#### IV. CONCLUSION

In this work, we provide two schemes to study how to achieve the remote entanglement between two mechanical nodes with resonant frequencies respectively in the megahertz and gigahertz ranges, which has been much less explored before. Specifically, based on the hybrid model which includes the dispersive and triple-resonant optomechanical couplings, we first discuss a protocol to achieve the megahertz-to-gigahertz entanglement distribution. This can be realized by activating the quantum entanglement in the local optomechanical system with megahertz mechanical mode and further redistribute it to the gigahertz mechanical mode via the optical photons transmission and the beam-splitter interaction activated in the distant optomechanical system. We also give a proposal to entangle two mechanical nodes over a long distance by using fast optical pulses, which suggests to redistribute the quantum entanglement generated in the optomechanical system with gigahertz mechanical mode to the remote optomechanical system with megahertz mechanical mode. In a word, this work shows the possibility of distinct mechanical nodes in the long-distance entanglement distribution, which may broaden the further application of different cavity optomechanical platforms and mechanical systems in hybrid quantum network, quantum information processing and fundamental physics test.

#### ACKNOWLEDGMENTS

We thank J. Li from Zhejiang University for helpful discussions and feedback. This work was supported by the Fundamental Research Program of Shanxi Province under Grant No. 202203021211260.

[1] T. D. Ladd, F. Jelezko, R. Laflamme, Y. Nakamura, C. Monroe, and J. L. O'Brien, Quantum computers, *Nature* **464**, 45 (2010).  
 [2] I. M. Georgescu, S. Ashhab, and F. Nori, Quantum simulation, *Rev. Mod. Phys.* **86**, 153 (2014).  
 [3] C. H. Bennett and D. P. DiVincenzo, Quantum information and computation, *Nature* **404**, 247 (2000).  
 [4] C. L. Degen, F. Reinhard, and P. Cappellaro, Quantum sensing, *Rev. Mod. Phys.* **89**, 035002 (2017).  
 [5] K. Azuma, S. E. Economou, D. Elkouss, P. Hilaire, L. Jiang, H.-K. Lo, and I. Tzitrin, Quantum repeaters: From quantum

networks to the quantum internet, *Rev. Mod. Phys.* **95**, 045006 (2023).  
 [6] H. J. Kimble, The quantum internet, *Nature* **453**, 1023 (2008).  
 [7] S. Wehner, D. Elkouss, and R. Hanson, Quantum internet: A vision for the road ahead, *Science* **362**, 303 (2018).  
 [8] G. Kurizki, P. Bertet, Y. Kubo, K. Mølmer, D. Petrosyan, P. Rabl, and J. Schmiedmayer, Quantum technologies with hybrid systems, *Proc. Natl. Acad. Sci. U.S.A.* **112**, 3866 (2015).  
 [9] A. A. Clerk, K. W. Lehnert, P. Bertet, J. R. Petta, and Y. Nakamura, Hybrid quantum systems with circuit quantum electrodynamics, *Nat. Phys.* **16**, 257 (2020).

- [10] M. Aspelmeyer, T. J. Kippenberg, and F. Marquardt, Cavity optomechanics, *Rev. Mod. Phys.* **86**, 1391 (2014).
- [11] R. Riedinger, S. Hong, R. A. Norte, J. A. Slater, J. Shang, A. G. Krause, V. Anant, M. Aspelmeyer, and S. Gröblacher, Non-classical correlations between single photons and phonons from a mechanical oscillator. *Nature* **530**, 313 (2016).
- [12] S. Hong, R. Riedinger, I. Marinković, A. Wallucks, S. G. Hofer, R. A. Norte, M. Aspelmeyer, and S. Gröblacher, Hanbury Brown and Twiss interferometry of single phonons from an optomechanical resonator, *Science* **358**, 203 (2017).
- [13] I. Marinković, A. Wallucks, R. Riedinger, S. Hong, M. Aspelmeyer, and S. Gröblacher, Optomechanical Bell Test, *Phys. Rev. Lett.* **121**, 220404 (2018).
- [14] N. Fiaschi, B. Hensen, A. Wallucks, R. Benevides, J. Li, T. P. Mayer Alegre, and S. Gröblacher, Optomechanical quantum teleportation, *Nat. Photonics* **15**, 817 (2021).
- [15] T. A. Palomaki, J. D. Teufel, R. W. Simmonds, and K. W. Lehnert, Entangling mechanical motion with microwave fields. *Science* **342**, 710 (2013).
- [16] E. E. Wollman, C. U. Lei, A. J. Weinstein, J. Suh, A. Kronwald, F. Marquardt, A. A. Clerk, and K. C. Schwab, Quantum squeezing of motion in a mechanical resonator, *Science* **349**, 952 (2015).
- [17] J.-M. Pirkkalainen, E. Damskäg, M. Brandt, F. Massel, and M. A. Sillanpää, Squeezing of quantum noise of motion in a micromechanical resonator, *Phys. Rev. Lett.* **115**, 243601 (2015).
- [18] F. Lecocq, J. B. Clark, R. W. Simmonds, J. Aumentado, and J. D. Teufel, Quantum nondemolition measurement of a nonclassical state of a massive object. *Phys. Rev. X* **5**, 041037 (2015).
- [19] J. Chan, T. P. M. Alegre, A. H. Safavi-Naeini, J. T. Hill, A. Krause, S. Gröblacher, M. Aspelmeyer, and O. Painter, Laser cooling of a nanomechanical oscillator into its quantum ground state, *Nature* **478**, 89 (2011).
- [20] J. D. Teufel, T. Donner, D. Li, J. W. Harlow, M. S. Allman, K. Cicak, A. J. Sirois, J. D. Whittaker, K. W. Lehnert, and R. W. Simmonds, Sideband cooling of micromechanical motion to the quantum ground state, *Nature* **475**, 359 (2011).
- [21] M. Rossi, D. Mason, J. Chen, Y. Tsaturyan, and A. Schliesser, Measurement-based quantum control of mechanical motion, *Nature* **563**, 53 (2018).
- [22] J. B. Clark, F. Lecocq, R. W. Simmonds, J. Aumentado, and J. D. Teufel, Sideband cooling beyond the quantum backaction limit with squeezed light, *Nature* **541**, 191 (2017).
- [23] Y.-S. Park and H. Wang, Resolved-sideband and cryogenic cooling of an optomechanical resonator, *Nat. Phys.* **5**, 489 (2009).
- [24] A. Schliesser, R. Rivière, G. Anetsberger, O. Arcizet, and T. J. Kippenberg, Resolved-sideband cooling of a micromechanical oscillator, *Nat. Phys.* **4**, 415 (2008).
- [25] Uroš Delić, M. Reisenbauer, K. Dare, D. Grass, V. Vuletić, N. Kiesel, M. Aspelmeyer, Cooling of a levitated nanoparticle to the motional quantum ground state, *Science* **367**, 892 (2020).
- [26] J. Li, S. Gröblacher, S.-Y. Zhu, and G. S. Agarwal, Generation and detection of non-Gaussian phonon-added coherent states in optomechanical systems, *Phys. Rev. A* **98**, 011801 (2018).
- [27] G.ENZIAN, J. J. Price, L. Freisem, J. Nunn, J. Janousek, B. C. Buchler, P. K. Lam, and M. R. Vanner, Single-Phonon Addition and Subtraction to a Mechanical Thermal State, *Phys. Rev. Lett.* **126**, 033601 (2021).
- [28] G.ENZIAN, L. Freisem, J. J. Price, A. Ø. Svela, J. Clarke, B. Shajilal, J. Janousek, B. C. Buchler, P. K. Lam, and M. R. Vanner, Non-Gaussian Mechanical Motion via Single and Multiphonon Subtraction from a Thermal State, *Phys. Rev. Lett.* **127**, 243601 (2021).
- [29] I. Shomroni, L. Qiu, and T. J. Kippenberg, Optomechanical generation of a mechanical catlike state by phonon subtraction, *Phys. Rev. A* **101**, 033812 (2020).
- [30] S. Pirandola, D. Vitali, P. Tombesi, and S. Lloyd, Macroscopic Entanglement by Entanglement Swapping, *Phys. Rev. Lett.* **97**, 150403 (2006).
- [31] M. J. Hartmann and M. B. Plenio, Steady State Entanglement in the Mechanical Vibrations of Two Dielectric Membranes, *Phys. Rev. Lett.* **101**, 200503 (2008).
- [32] C. Joshi, J. Larson, M. Jonson, E. Andersson, and P. Öhberg, Entanglement of distant optomechanical systems, *Phys. Rev. A* **85**, 033805 (2012).
- [33] Y.-D. Wang and A. A. Clerk, Reservoir-Engineered Entanglement in Optomechanical Systems, *Phys. Rev. Lett.* **110**, 253601 (2013).
- [34] J.-Q. Liao, Q.-Q. Wu, and F. Nori, Entangling two macroscopic mechanical mirrors in a two-cavity optomechanical system, *Phys. Rev. A* **89**, 014302 (2014).
- [35] C.-J. Yang, J.-H. An, W. Yang, and Y. Li, Generation of stable entanglement between two cavity mirrors by squeezed-reservoir engineering, *Phys. Rev. A* **92**, 062311 (2015).
- [36] M. Wang, X.-Y. Lü, Y.-D. Wang, J. Q. You, and Y. Wu, Macroscopic quantum entanglement in modulated optomechanics, *Phys. Rev. A* **94**, 053807 (2016).
- [37] R.-X. Chen, C.-G. Liao, and X.-M. Lin, Dissipative generation of significant amount of mechanical entanglement in a coupled optomechanical system, *Sci. Rep.* **7**, 14497 (2017).
- [38] S. Chakraborty and A. K. Sarma, Entanglement dynamics of two coupled mechanical oscillators in modulated optomechanics, *Phys. Rev. A* **97**, 022336 (2018).
- [39] C.-S. Hu, X.-Y. Lin, L.-T. Shen, W.-J. Su, Y.-K. Jiang, H. Wu, and S.-B. Zheng, Improving macroscopic entanglement with nonlocal mechanical squeezing, *Opt. Express* **28**, 1492 (2020).
- [40] J. Clarke, P. Sahium, K. E. Khosla, I. Pikovski, M. S. Kim, and M. R. Vanner, Generating mechanical and optomechanical entanglement via pulsed interaction and measurement, *New J. Phys.* **22**, 063001 (2020).
- [41] Y. Li, L. Deng, T. Yin, and A. Chen, Entanglement Between Two Mechanical Oscillators in a Dual-Coupling Optomechanical System, *Front. Phys.* **10**, 908205 (2022).
- [42] Y.-F. Jiao, Y.-L. Zuo, Y. Wang, W. Lu, J.-Q. Liao, L.-M. Kuang, and H. Jing, Tripartite Quantum Entanglement with Squeezed Optomechanics. *Laser Photonics Rev.* **18**, 2301154 (2024).
- [43] R. Riedinger, A. Wallucks, I. Marinković, C. Löschnauer, M. Aspelmeyer, S. Hong, and S. Gröblacher, Remote quantum entanglement between two micromechanical oscillators. *Nature* **556**, 473 (2018).
- [44] C. F. Ockeloen-Korppi, E. Damskäg, J.-M. Pirkkalainen, M. Asjad, A. A. Clerk, F. Massel, M. J. Woolley, and M. A. Sillanpää, Stabilized entanglement of massive mechanical oscillators. *Nature* **556**, 478 (2018).
- [45] L. M. De Lépinay, C. F. Ockeloen-Korppi, M. J. Woolley, and M. A. Sillanpää, Quantum mechanics-free subsystem with mechanical oscillators. *Science* **372**, 625 (2021).
- [46] S. Kotler, G. A. Peterson, E. Shojaei, F. Lecocq, K. Cicak, A. Kwiatkowski, S. Geller, S. Glancy, E. Knill, R. W. Simmonds, J. Aumentado, J. D. Teufel, Direct observation of deterministic macroscopic entanglement. *Science* **372**, 622 (2021).
- [47] M. Forsch, R. Stockill, A. Wallucks, I. Marinković, C. Gärtner, R. A. Norte, F. van Otten, A. Fiore, K. Srinivasan, and S. Gröblacher, Microwave-to-optics conversion using a mechanical oscillator in its quantum ground state. *Nat. Phys.* **16**, 69 (2019).

- [48] M. Mirhosseini, A. Sipahigil, M. Kalae, and O. Painter, Superconducting qubit to optical photon transduction, *Nature* **588**, 599 (2020).
- [49] V. Fiore, Y. Yang, M. C. Kuzyk, R. Barbour, L. Tian, and H. Wang, Storing Optical Information as a Mechanical Excitation in a Silica Optomechanical Resonator, *Phys. Rev. Lett.* **107**, 133601 (2011).
- [50] A. Schliesser, O. Arcizet, R. Rivière, G. Anetsberger, and T. J. Kippenberg, Resolved-sideband cooling and position measurement of a micromechanical oscillator close to the Heisenberg uncertainty limit, *Nat. Phys.* **5**, 509 (2009).
- [51] J. B. Hertzberg, T. Rocheleau, T. Ndikum, M. Savva, A. A. Clerk and K. C. Schwab, Back-action-evading measurements of nanomechanical motion, *Nat. Phys.* **6**, 213 (2010).
- [52] C. F. Ockeloen-Korppi, E. Damskäg, J.-M. Pirkkalainen, A. A. Clerk, M. J. Woolley, and M. A. Sillanpää, Quantum back-action evading measurement of collective mechanical modes, *Phys. Rev. Lett.* **117**, 140401 (2016).
- [53] Z. Shen, Y.-L. Zhang, Y. Chen, C.-L. Zou, Y.-F. Xiao, X.-B. Zou, F.-W. Sun, G.-C. Guo, and C.-H. Dong, Experimental realization of optomechanically induced non-reciprocity, *Nat. Photonics* **10**, 657 (2016).
- [54] F. Ruesink, M.-A. Miri, A. Aù and E. Verhagen, Nonreciprocity and magnetic-free isolation based on optomechanical interactions, *Nat. Commun.* **7**, 13662 (2016).
- [55] N. R. Bernier, L. D. Tóth, A. Koottandavida, M. A. Ioannou, D. Malz, A. Nunnenkamp, A. K. Feofanov and T. J. Kippenberg, Nonreciprocal reconfigurable microwave optomechanical circuit, *Nat. Commun.* **8**, 604 (2017).
- [56] G. A. Peterson, F. Lecocq, K. Cicak, R. W. Simmonds, J. Aumentado and J. D. Teufel, Demonstration of efficient nonreciprocity in microwave optomechanical circuit, *Phys. Rev. X* **7**, 031001 (2017).
- [57] I. S. Grudinin, H. Lee, O. Painter and K. J. Vahala, Phonon Laser Action in a Tunable Two-Level System, *Phys. Rev. Lett.* **104**, 083901 (2010).
- [58] H. Jing, S. K. Özdemir, X.-Y. Lü, J. Zhang, L. Yang, and F. Nori, PT-Symmetric Phonon Laser, *Phys. Rev. Lett.* **113**, 053604 (2014).
- [59] J. Zhang, B. Peng, Ş. Kaya Özdemir, K. Pichler, D. O. Krimer, G. Zhao, F. Nori, Y. Liu, S. Rotter, and L. Yang, A phonon laser operating at an exceptional point, *Nat. Photonics* **12**, 479 (2018).
- [60] H. Tan, L. F. Buchmann, H. Seok, and G. Li, Achieving steady-state entanglement of remote micromechanical oscillators by cascaded cavity coupling, *Phys. Rev. A* **87**, 022318 (2013).
- [61] Y.-F. Jiao, J.-X. Liu, Y. Li, R. Yang, L.-M. Kuang, and H. Jing, Nonreciprocal Enhancement of Remote Entanglement between Nonidentical Mechanical Oscillators, *Phys. Rev. Appl.* **18**, 064008 (2022)
- [62] J. Li, I. M. Haghghi, N. Malossi, S. Zippilli, and D. Vitali, Generation and detection of large and robust entanglement between two different mechanical resonators in cavity optomechanics, *New J. Phys.* **17** 103037 (2015).
- [63] C.-H. Bai, D.-Y. Wang, S. Zhang, S. Liu, and H.-F. Wang, Generation of Strong Mechanical-Mechanical Entanglement by Pump Modulation, *Adv. Quantum Technol.* **4**, 2000149 (2021).
- [64] Z. Shen, G.-T. Xu, M. Zhang, Y.-L. Zhang, Y. Wang, C.-Z. Chai, C.-L. Zou, G.-C. Guo, and C.-H. Dong, Coherent Coupling between Phonons, Magnons, and Photons, *Phys. Rev. Lett.* **129**, 243601 (2022).
- [65] S. Weis, R. Rivière, S. Deléglise, E. Gavartin, O. Arcizet, A. Schliesser, and T. J. Kippenberg, Optomechanically induced transparency, *Science* **330**, 1520 (2010).
- [66] C. W. Gardiner and M. J. Collett, Input and output in damped quantum systems: Quantum stochastic differential equations and the master equation, *Phys. Rev. A* **31**, 3761 (1985).
- [67] U. Leonhardt, *Measuring the Quantum State of Light* (Cambridge University Press, UK, 1997).
- [68] J. Li, G. Li, J.-M. Wang, S.-Y. Zhu, and T.-C. Zhang, A comparison of two nonclassical measures, entanglement potential and the negativity of the Wigner function, *J. Phys. B: At. Mol. Opt. Phys.* **43**, 085504 (2010).
- [69] J. Li, Y.-P. Wang, W.-J. Wu, S.-Y. Zhu, and J.Q. You, Quantum Network with Magnonic and Mechanical Nodes, *PRX Quantum* **2**, 040344 (2021).
- [70] H. Tan, and J. Li, Einstein-Podolsky-Rosen entanglement and asymmetric steering between distant macroscopic mechanical and magnonic systems, *Phys. Rev. Res.* **3**, 013192 (2021).
- [71] V. Giovannetti and D. Vitali, Phase-noise measurement in a cavity with a movable mirror undergoing quantum Brownian motion, *Phys. Rev. A* **63**, 023812 (2001).
- [72] D. Vitali, S. Gigan, A. Ferreira, H. R. Bohm, P. Tombesi, A. Guerreiro, V. Vedral, A. Zeilinger, and M. Aspelmeyer, Optomechanical Entanglement between a Movable Mirror and a Cavity Field, *Phys. Rev. Lett.* **98**, 030405 (2007).
- [73] C. Genes, A. Mari, P. Tombesi, and D. Vitali, Robust entanglement of a micromechanical resonator with output optical fields, *Phys. Rev. A* **78**, 032316 (2008).
- [74] J. Li, S.-Y. Zhu, and G. S. Agarwal, Magnon-Photon-Phonon Entanglement in Cavity Magnomechanics, *Phys. Rev. Lett.* **121**, 203601 (2018).
- [75] T. J. Kippenberg and K. J. Vahala, Cavity Optomechanics: Back-Action at the Mesoscale, *Science* **321**, 1172 (2008).
- [76] M. Aspelmeyer, S. Gröblacher, K. Hammerer, and N. Kiesel, Quantum optomechanics-throwing a glance, *J. Opt. Soc. Am. B* **27**, A189 (2010).
- [77] G. Adesso, A. Serafini, and F. Illuminati, Extremal entanglement and mixedness in continuous variable systems, *Phys. Rev. A* **70**, 022318 (2004).
- [78] S. G. Hofer, W. Wieczorek, M. Aspelmeyer, and K. Hammerer, Quantum entanglement and teleportation in pulsed cavity optomechanics, *Phys. Rev. A* **84**, 052327 (2011).
- [79] C. Galland, N. Sangouard, N. Piro, N. Gisin, and T. J. Kippenberg, Heralded Single-Phonon Preparation, Storage, and Readout in Cavity Optomechanics, *Phys. Rev. Lett.* **112**, 143602 (2014).
- [80] Z.-X. Lu, X. Zuo, Z.-Y. Fan, and J. Li, Optomagnonic continuous-variable quantum teleportation enhanced by non-Gaussian distillation, *Phys. Rev. Res.* **7**, 043148 (2025).
- [81] S. M. Meenehan, J. D. Cohen, G. S. MacCabe, F. Marsili, M. D. Shaw, and O. Painter, Pulsed Excitation Dynamics of an Optomechanical Crystal Resonator near Its Quantum Ground State of Motion, *Phys. Rev. X* **5**, 041002 (2015).
- [82] E. Verhagen, S. Deléglise, S. Weis, A. Schliesser, and T. J. Kippenberg, Quantum-coherent coupling of a mechanical oscillator to an optical cavity mode, *Nature* **482**, 63 (2012).